Kolmogorov flow: Linear stability and energy transfers in a minimal low-dimensional model

Cite as: Chaos **30**, 073110 (2020); https://doi.org/10.1063/5.0002751
Submitted: 27 January 2020 . Accepted: 16 June 2020 . Published Online: 06 July 2020

Soumyadeep Chatterjee, and Mahendra K. Verma

Kolmogorov flow: Linear stability and energy transfers in a minimal low-dimensional model

Cite as: Chaos **30**, 073110 (2020); doi: 10.1063/5.0002751
Submitted: 27 January 2020 · Accepted: 16 June 2020 ·
Published Online: 6 July 2020

View Online Export Citation CrossMark

Soumyadeep Chatterjee[a] and Mahendra K. Verma[b]

AFFILIATIONS

Department of Physics, Indian Institute of Technology Kanpur, Kanpur 208016, India

[a]**Author to whom correspondence should be addressed:** soumyade@iitk.ac.in
[b]**Electronic mail:** mkv@iitk.ac.in

ABSTRACT

In this paper, we derive a four-mode model for the Kolmogorov flow by employing Galerkin truncation and the Craya–Herring basis for the decomposition of velocity field. After this, we perform a bifurcation analysis of the model. Though our low-dimensional model has fewer modes than past models, it captures the essential features of the primary bifurcation of the Kolmogorov flow. For example, it reproduces the critical Reynolds number for the supercritical pitchfork bifurcation and the flow structures of past works. We also demonstrate energy transfers from intermediate scales to large scales. We perform direct numerical simulations of the Kolmogorov flow and show that our model predictions match the numerical simulations very well.

In the late 1950s, Kolmogorov urged the fluid community to explore the stability criteria of a shear flow with spatially periodic forcing, a system referred to as the Kolmogorov flow. Since then, many researchers have attempted to address the above problem using analytical, numerical, and experimental tools. The leading analytical results involve infinite or a large number of interacting Fourier modes. The numerical calculations and low-dimensional models also involve many Fourier modes. In this paper, we construct a four-mode low-dimensional model using Galerkin truncation and the Craya–Herring basis. Our minimal model of the Kolmogorov flow captures the essential features of its primary bifurcation and the critical Reynolds number very well. The model predictions are borne out in numerical simulations.

I. INTRODUCTION

Flow instability and transition to turbulence are important problems of fluid dynamics. Kolmogorov abstracted a simple shear flow with spatially periodic forcing,[1–3] whose instability and bifurcation have been studied intensely over the years. Also, the Kolmogorov flow has been experimentally realized in several setups, including a soap film[4] and an electrolytic fluid.[5,6] In this paper, we analyze the stability of the Kolmogorov flow using a low-dimensional model consisting of four Fourier modes. We validate the model using numerical solutions.

Meshalkin and Sinai[7] provided the first solution to the stability of the Kolmogorov flow. They considered an external force per unit mass, $\gamma \sin k_f y\, \hat{x}$, where γ is the force amplitude and k_f is the force wavenumber. Meshalkin and Sinai[7] considered $k_f = 1$ and analyzed the stability of the two-dimensional flow with $L_x/L_y = 1/\alpha$. They considered small perturbation on the fundamental stream function (corresponding to the external force) and focused on its time variations. They incorporated the effects of all Fourier modes and studied the stability problem with continued fractions. An outcome of their analysis is that, for $\alpha < 1$, the laminar solution becomes unstable at the critical Reynolds number R_c and $R_c \to \sqrt{2}$ (for normalization of Iudovich[8]) as $\alpha \to 0$. They observed that the laminar solution is stable for $\alpha > 1$. Using an asymptotic instability analysis, Sivashinsky[9] showed that a periodically forced two-dimensional plane-parallel flow becomes unstable beyond a critical Reynolds number. He showed the secondary flow to be chaotically self-fluctuating.

Iudovich[8] and Marchioro[10] extended the calculation of Meshalkin and Sinai[7] and concluded that the laminar flow is globally stable for $\alpha \geq 1$. For $\alpha < 1$, Iudovich[8] proved that $R_c \to \sqrt{2}$ for $\alpha \to 0$ and $R_c \to \infty$ when $\alpha \to 1$. They showed that R_c increases monotonically with α between $R_c = \sqrt{2}$ for $\alpha \to 0$ and $R_c = \infty$ for $\alpha \to 1$. The R_c curve represents neutral stability.

Okamoto and Shōji[11] performed a bifurcation analysis of the Kolmogorov flow with a finite set of Fourier modes and showed supercritical pitchfork to be the primary bifurcation. They considered 544 modes for $\alpha > 0.3$, even more modes for $\alpha < 0.3$, and observed that $R_c = 3.011\,193$ for $\alpha = 0.7$. Using more sophisticated calculation, Nagatou[12] reported R_c to be bracketed between 3.011 528 364 444 and 3.011 528 364 446. Later, Okamoto[13,14] extended the bifurcation diagram to larger R using the path-continuation method. Matsuda and Miyatake[15] studied the bifurcation diagram further and derived an exact formula for the second derivatives of their components at the bifurcation points.

The Kolmogorov flow has been simulated in experiments by inducing vortices in magnetofluids using periodically placed electrodes. Tabeling, Perrin, and Fauve[16] observed supercritical pitchfork bifurcation at the instability of the vortices. Bondarenko, Gak, and Dolzhanskii[5] performed a similar experiment. In another experiment, Sommeria[17] reported the existence of an inverse cascade due to the nonlinear interactions. Herault, Pétrélis, and Fauve[18] observed $1/f$ noise in the nonlinear regime of the Kolmogorov flow. Tabeling[19] reviewed the experiments related to the Kolmogorov flow.

Gotoh and Yamada[20] performed instability analysis of the rhombic cells with the stream function as $\cos kx + \cos y$, where k is the aspect ratio of the cell. Kim and Okamoto[21] performed bifurcation and inviscid limit analysis for the aforementioned rhombic cells. Thess[22] studied the effects of viscosity, linear friction, and confinement on the flow. Platt, Sirovich, and Fitzmaurice[23] analyzed the Kolmogorov flow for $k_f = 4$ and observed a sequence of bifurcations leading to chaos. For the same k_f, Chen and Price[24] studied the chaotic behavior using a truncation model with nine modes. In addition, researchers have studied variations of the Kolmogorov flow to three-dimensional flows.[25]

The Kolmogorov flow is useful not only for analyzing transition to turbulence but also for studying the inverse cascade in two-dimensional turbulence.[26–28] Green[26] reported that for $k > k_f$, kinetic energy spectrum, $E(k) \sim k^{-5}$, whereas for $k < k_f$, $E(k) \sim k$. Sommeria[17] studied the inverse cascade experimentally and reported the exponent to be in the range of -4.5 to -4.9 for $k > k_f$. For $k < k_f$, direct numerical simulations (DNSs) reveal that $E(k) \sim k^{-5/3}$. For random forcing in a wavenumber band near $k = k_f$, Gupta *et al.*[27] showed that for $k > k_f$, the energy spectrum is of the form $k^{-3}\exp(-k^2)$; the exponential part gives an appearance of a steeper spectrum compared to k^{-3}. Zhang *et al.*[28] performed a molecular simulation using the Fokker–Planck method and reported that $E(k) \sim k^{-4}$ for $k < k_f$ due to condensation in the large-scale structures. For $k > k_f$, Zhang *et al.*[28] reported that $E(k) \sim \exp(-0.2k)$. Energy condensate is observed at the large scale due to an inverse cascade. Gallet and Young[29] derived a mathematical model of energy condensation in the absence of large-scale dissipation. Mishra *et al.*[30] studied the condensate regime using Ekman friction. There are more works on the Kolmogorov flow, including those by Chandler and Kerswell,[31] Lucas and Kerswell,[32] and Fylladitakis,[33] and references therein.

In this paper, we consider incompressible Kolmogorov flow in a two-dimensional periodic box with the aspect ratio α and construct a low-dimensional model with four modes. We perform bifurcation analysis of the system and derive the critical Reynolds number for the instability. Our results are consistent with previous results. Besides, we also carry out direct numerical simulations of the Kolmogorov flow for the parameter used for our model. The results from these simulations are in good agreement with those from the low-dimensional model. These results give us confidence that the chosen modes are a good choice for the Kolmogorov flow.

The outline of this paper is as follows. In Sec. II, we present the governing equations and the low-dimensional model. In Sec. III, we perform linear stability and bifurcation analysis of the low-dimensional model. We describe the energy transfers among the participating modes in Sec. IV. In Sec. V, we present numerical validation using direct numerical simulation. We conclude in Sec. VI.

II. BASIC FORMULATION

For an incompressible flow, the Navier–Stokes equation and incompressibility condition[34,35] are

$$\frac{\partial \mathbf{u}}{\partial t} + \mathbf{u}\cdot\nabla\mathbf{u} = -\nabla p + \mathbf{F}_u + \nu\nabla^2\mathbf{u}, \tag{1}$$

$$\nabla\cdot\mathbf{u} = 0, \tag{2}$$

where $\mathbf{u}$ and p are the velocity and pressure fields, respectively, ν is the kinematic viscosity, and $\mathbf{F}_u$ is the acceleration due to the external force. We consider a two-dimensional Kolmogorov flow in a doubly periodic box of size $L_x \times L_y$. The ratio $\alpha = L_y/L_x$ is called the aspect ratio. We assume density ρ to be unity. We take

$$\mathbf{F}_u = \gamma \sin\left(\frac{2\pi y k_f}{L_y}\right)\hat{x}, \tag{3}$$

where γ is the amplitude of the acceleration and k_f is the forcing wavenumber which we consider to be 1.

We nondimensionalize Eqs. (1) and (2) using $L_y/2\pi$ as the length scale and $2\pi\nu/\gamma L_y$ as the time scale and obtain the following equations:

$$\frac{\partial \mathbf{u}}{\partial t} + \mathbf{u}\cdot\nabla\mathbf{u} = -\nabla p + \frac{1}{R}\sin(y)\hat{x} + \frac{1}{R}\nabla^2\mathbf{u}, \tag{4}$$

$$\nabla\cdot\mathbf{u} = 0, \tag{5}$$

where

$$R = \frac{\gamma}{\nu^2}\left(\frac{L_y}{2\pi}\right)^3 \tag{6}$$

is the Reynolds number. A trivial stationary solution of Eqs. (4) and (5) is

$$\mathbf{u} = (\sin(y), 0), \quad p = \text{const.} \tag{7}$$

This solution represents a laminar flow.

For stability analysis, it is customary to work in a Fourier space. In this space, the equations get transformed to

$$\frac{d}{dt}\mathbf{u}(\mathbf{k}) + \mathbf{N}_\mathbf{u}(\mathbf{k}) = -i\mathbf{k}p(\mathbf{k}) + \mathbf{F}_u(\mathbf{k}) - \frac{1}{R}k^2\mathbf{u}(\mathbf{k}), \tag{8}$$

$$\mathbf{k}.\mathbf{u}(\mathbf{k}) = 0, \tag{9}$$

where

$$\mathbf{N_u}(\mathbf{k}) = i\sum_{\mathbf{p}}\{\mathbf{k}\cdot\mathbf{u}(-\mathbf{q})\}\mathbf{u}(-\mathbf{p}), \tag{10}$$

$$p(\mathbf{k}) = \frac{i}{k^2}\mathbf{k}\cdot[\mathbf{N_u}(\mathbf{k}) - \mathbf{F_u}(\mathbf{k})] \tag{11}$$

are the Fourier transforms of the nonlinear and pressure terms, respectively. Here, $\mathbf{k} = -\mathbf{p} - \mathbf{q}$. Note that calculation of $\mathbf{N_u}(\mathbf{k})$ requires all possible wavenumber triads. We denote the Fourier mode as $\mathbf{k} = (\alpha l, m)$, where l, m are integers.

The Fourier transform of the external force $\frac{1}{R}\sin(y)\hat{x}$ is

$$\mathbf{F}_u(\mathbf{k}) = \frac{1}{2iR}[\delta_{k_y,1} - \delta_{k_y,-1}]\hat{x}. \tag{12}$$

That is, the forcing wavenumbers are $(0,1)$ and $(0,-1)$. Near the onset of instability, the nonlinear term $\mathbf{u}\cdot\nabla\mathbf{u}$ generates other Fourier modes. In this paper, we show that a low-dimensional model having nonzero Fourier modes at wavenumbers $\{\mathbf{k} = (-\alpha, 0), \mathbf{p} = (0,1), \mathbf{q} = (\alpha, -1)$, and $\mathbf{s} = (\alpha, 1)\}$ reproduces earlier results on the Kolmogorov flow quite well (e.g., Iudovich[8]). In Sec. V, we perform direct numerical simulations and show that our low-dimensional model reproduces the simulation results to a significant degree. Due to these reasons, we work with this set of Fourier modes. We consider the following interacting triads:

$$\mathbf{k}\bigoplus\mathbf{p}\bigoplus\mathbf{q} = (-\alpha,0)\bigoplus(0,1)\bigoplus(\alpha,-1) = 0, \tag{13}$$

$$(-\mathbf{k})\bigoplus\mathbf{p}\bigoplus(-\mathbf{s}) = (\alpha,0)\bigoplus(0,1)\bigoplus(-\alpha,-1) = 0, \tag{14}$$

where $\bigoplus$ represents a nonlinear interaction (see Fig. 1). Thus, possible nonlinear interactions for the modes with wavenumbers $\mathbf{k}$, $\mathbf{p}$, $\mathbf{q}$, and $\mathbf{s}$ are

$$\mathbf{k} = [(-\alpha,-1)\bigoplus(0,1)] + [(-\alpha,1)\bigoplus(0,-1)], \tag{15}$$

$$\mathbf{p} = [(-\alpha,0)\bigoplus(\alpha,1)] + [(\alpha,0)\bigoplus(-\alpha,1)], \tag{16}$$

$$\mathbf{q} = [(\alpha,0)\bigoplus(0,-1)], \tag{17}$$

$$\mathbf{s} = [(\alpha,0)\bigoplus(0,1)]. \tag{18}$$

In Sec. III, we derive the governing equations for the above Fourier modes.

III. LINEAR STABILITY AND BIFURCATION ANALYSIS

The derivation of the evolution equations for the Fourier modes gets simplified in the Craya–Herring basis.[35–39] For the wavenumber $\mathbf{k}$, the unit vectors in this basis are[35–39]

$$\hat{e}_3(\mathbf{k}) = \hat{k}, \tag{19}$$

$$\hat{e}_1(\mathbf{k}) = \frac{\hat{k}\times\hat{n}}{|\hat{k}\times\hat{n}|}, \tag{20}$$

$$\hat{e}_2(\mathbf{k}) = \hat{e}_3(\mathbf{k})\times\hat{e}_1(\mathbf{k}), \tag{21}$$

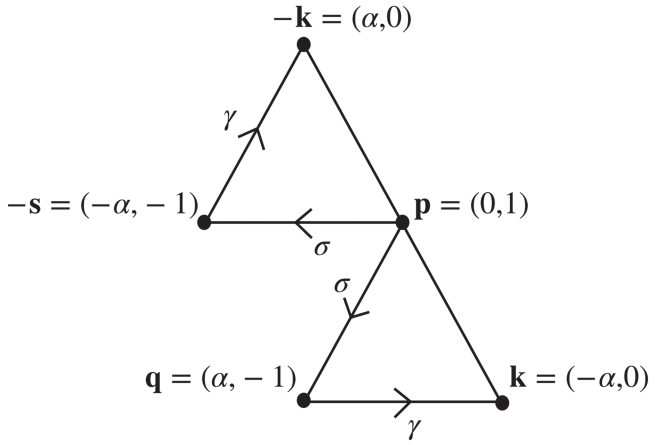

FIG. 1. Schematic representation of the triad interactions in Eqs. (13) and (14). Energy transfers σ and γ are $(r-1)/(4\sqrt{2}Rr^2)$ and $(\alpha^2(r-1))/(4\sqrt{2}Rr^2)$, where $r = R/R_c$.

where $\hat{k}$ is the unit vector along $\mathbf{k}$ and $\hat{n} = \hat{z}$. For all the wavenumbers under consideration, $\hat{e}_1$ lies on the plane, while $\hat{e}_2$ is perpendicular to the plane. Hence, for the present 2D flow, $u_2 = 0$ for all the modes. In addition, $u_3 = 0$ due to incompressibility condition [Eq. (9)]. Therefore,

$$\mathbf{u}(\mathbf{k}) = u_1(\mathbf{k})\hat{e}_1(\mathbf{k}). \tag{22}$$

Explicitly, the unit vectors $\hat{e}_1$'s for the four wavenumbers ($\mathbf{k}$,$\mathbf{p}$, $\mathbf{q}$, $\mathbf{s}$) are

$$\hat{e}_1(\mathbf{k}) = \hat{y}, \tag{23}$$

$$\hat{e}_1(\mathbf{p}) = \hat{x}, \tag{24}$$

$$\hat{e}_1(\mathbf{q}) = -\frac{1}{\sqrt{\alpha^2+1}}\hat{x} - \frac{\alpha}{\sqrt{\alpha^2+1}}\hat{y}, \tag{25}$$

$$\hat{e}_1(\mathbf{s}) = \frac{1}{\sqrt{\alpha^2+1}}\hat{x} - \frac{\alpha}{\sqrt{\alpha^2+1}}\hat{y}. \tag{26}$$

Using Eqs. (23)–(26), we derive the evolution equations for u_1's as

$$\frac{d}{dt}u_1(\mathbf{k}) = -\left(\frac{\alpha^2}{\sqrt{1+\alpha^2}}i\right)(u_1^*(\mathbf{p})u_1^*(\mathbf{q}) + u_1^*(\mathbf{s})u_1(\mathbf{p})) - \left(\frac{\alpha^2}{R}\right)u_1(\mathbf{k}), \tag{27}$$

$$\frac{d}{dt}u_1(\mathbf{p}) = \left(\frac{1}{\sqrt{1+\alpha^2}}i\right)(u_1^*(\mathbf{k})u_1^*(\mathbf{q}) - u_1(\mathbf{k})u_1(\mathbf{s})) + \frac{1}{2iR} - \left(\frac{1}{R}\right)u_1(\mathbf{p}), \tag{28}$$

$$\frac{d}{dt}u_1(\mathbf{q}) = -\left(\frac{1-\alpha^2}{\sqrt{1+\alpha^2}}i\right)u_1^*(\mathbf{k})u_1^*(\mathbf{p}) - \left(\frac{1+\alpha^2}{R}\right)u_1(\mathbf{q}), \tag{29}$$

$$\frac{d}{dt}u_1(\mathbf{s}) = -\left(\frac{1-\alpha^2}{\sqrt{1+\alpha^2}}i\right)u_1^*(\mathbf{k})u_1(\mathbf{p}) - \left(\frac{1+\alpha^2}{R}\right)u_1(\mathbf{s}). \tag{30}$$

The steady-state solutions of the above equations are

$$S_0 : \begin{cases} u_1(\mathbf{k}) = 0, \\ u_1(\mathbf{p}) = \frac{1}{2i}, \\ u_1(\mathbf{q}) = 0, \\ u_1(\mathbf{s}) = 0, \end{cases} \tag{31}$$

$$S_1 : \begin{cases} u_1(\mathbf{k}) = -\frac{1}{\sqrt{2}r}\sqrt{r-1}, \\ u_1(\mathbf{p}) = -\frac{1}{2r}i, \\ u_1(\mathbf{q}) = -\frac{\sqrt{1+\alpha^2}}{2R}\sqrt{r-1}, \\ u_1(\mathbf{s}) = \frac{\sqrt{1+\alpha^2}}{2R}\sqrt{r-1}, \end{cases} \tag{32}$$

and

$$S_2 : \begin{cases} u_1(\mathbf{k}) = \frac{1}{\sqrt{2}r}\sqrt{r-1}, \\ u_1(\mathbf{p}) = -\frac{1}{2r}i, \\ u_1(\mathbf{q}) = \frac{\sqrt{1+\alpha^2}}{2R}\sqrt{r-1}, \\ u_1(\mathbf{s}) = -\frac{\sqrt{1+\alpha^2}}{2R}\sqrt{r-1}, \end{cases} \tag{33}$$

where $r = R/R_c$ with

$$R_c = \frac{\sqrt{2}(1+\alpha^2)}{\sqrt{1-\alpha^2}}. \tag{34}$$

The solution S_0 is valid for all r, while S_1 and S_2 are defined only for $r > 1$. Also, $u_1(\mathbf{k}), u_1(\mathbf{q}), u_1(\mathbf{s})$ modes of S_1 have opposite signs compared to S_2. See Fig. 2 for an illustration of steady $u_1(\mathbf{k})$ for $\alpha = 0.7$; the figure exhibits a transition from S_0 to S_1 or S_2 at $r = 1$. For $r > 1$, the system follows either the S_1 branch or the S_2 branch depending on the initial condition. In Subsections III A and III B, we show that S_0 is the only stable solution for $r < 1$, while S_1 and S_2 are the stable solutions for $r > 1$. For $r > 1$, the solution S_0 is unstable. Another important point to note that R_c, S_1, S_2 are not defined for $\alpha > 1$; hence, S_0 is the only solution for $\alpha > 1$.

In Subsections III A and III B, we analyze the stability of S_0, S_1, and S_2.

A. Stability of the laminar solution S_0

First, we analyze the stability of the laminar solution, S_0. For the same, we linearize Eqs. (27)–(30) around S_0 and obtain the following equations:

$$\frac{d}{dt}\tilde{u}_1(\mathbf{k}) = -\left(\frac{\alpha^2}{2\sqrt{1+\alpha^2}}\right)(\tilde{u}_1^*(\mathbf{s}) - \tilde{u}_1^*(\mathbf{q})) - \left(\frac{\alpha^2}{R}\right)\tilde{u}_1(\mathbf{k}), \tag{35}$$

$$\frac{d}{dt}\tilde{u}_1(\mathbf{p}) = -\frac{1}{R}\tilde{u}_1(\mathbf{p}), \tag{36}$$

$$\frac{d}{dt}\tilde{u}_1(\mathbf{q}) = \left(\frac{(1-\alpha^2)}{2\sqrt{1+\alpha^2}}\right)\tilde{u}_1^*(\mathbf{k}) - \left(\frac{1+\alpha^2}{R}\right)\tilde{u}_1(\mathbf{q}), \tag{37}$$

$$\frac{d}{dt}\tilde{u}_1(\mathbf{s}) = -\left(\frac{(1-\alpha^2)}{2\sqrt{1+\alpha^2}}\right)\tilde{u}_1^*(\mathbf{k}) - \left(\frac{1+\alpha^2}{R}\right)\tilde{u}_1(\mathbf{s}), \tag{38}$$

where $\tilde{u}_1(\mathbf{k})$, $\tilde{u}_1(\mathbf{p})$, $\tilde{u}_1(\mathbf{q})$, and $\tilde{u}_1(\mathbf{s})$ represent fluctuations in S_0, and they are complex quantities. Hence, we split them into real and imaginary parts,

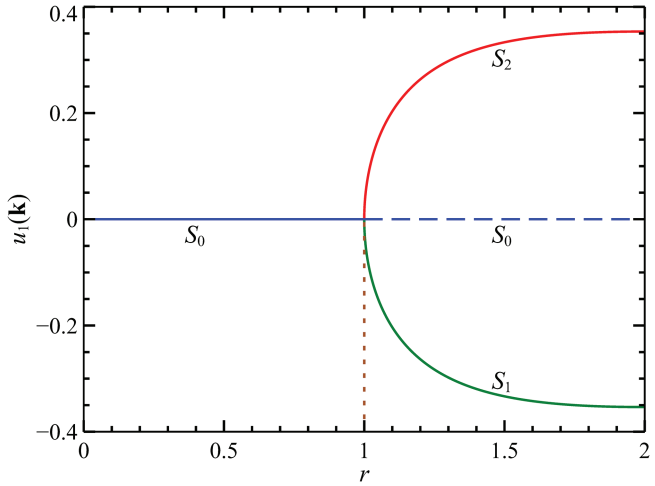

FIG. 2. For $\alpha = 0.7$, $u_1(\mathbf{k})$ as a function of r.

$$\tilde{u}_1(\mathbf{k}) = \Re[\tilde{u}_1(\mathbf{k})] + i\Im[\tilde{u}_1(\mathbf{k})], \tag{39}$$

$$\tilde{u}_1(\mathbf{p}) = \Re[\tilde{u}_1(\mathbf{p})] + i\Im[\tilde{u}_1(\mathbf{p})], \tag{40}$$

$$\tilde{u}_1(\mathbf{q}) = \Re[\tilde{u}_1(\mathbf{q})] + i\Im[\tilde{u}_1(\mathbf{q})], \tag{41}$$

$$\tilde{u}_1(\mathbf{s}) = \Re[\tilde{u}_1(\mathbf{s})] + i\Im[\tilde{u}_1(\mathbf{s})]. \tag{42}$$

Using Eqs. (35)–(38), we derive the following matrix equation:

$$\frac{d}{dt}\mathbb{U} = \mathbb{A}\mathbb{U}, \tag{43}$$

where

$$\mathbb{A} = \begin{pmatrix} -\frac{A}{R} & 0 & 0 & 0 & B & 0 & -B & 0 \\ 0 & -\frac{A}{R} & 0 & 0 & 0 & -B & 0 & B \\ 0 & 0 & -\frac{1}{R} & 0 & 0 & 0 & 0 & 0 \\ 0 & 0 & 0 & -\frac{1}{R} & 0 & 0 & 0 & 0 \\ D & 0 & 0 & 0 & -\frac{C}{R} & 0 & 0 & 0 \\ 0 & -D & 0 & 0 & 0 & -\frac{C}{R} & 0 & 0 \\ -D & 0 & 0 & 0 & 0 & 0 & -\frac{C}{R} & 0 \\ 0 & D & 0 & 0 & 0 & 0 & 0 & -\frac{C}{R} \end{pmatrix},$$

$$\mathbb{U} = \begin{pmatrix} \Re[\tilde{u}_1(\mathbf{k})] \\ \Im[\tilde{u}_1(\mathbf{k})] \\ \Re[\tilde{u}_1(\mathbf{p})] \\ \Im[\tilde{u}_1(\mathbf{p})] \\ \Re[\tilde{u}_1(\mathbf{q})] \\ \Im[\tilde{u}_1(\mathbf{q})] \\ \Re[\tilde{u}_1(\mathbf{s})] \\ \Im[\tilde{u}_1(\mathbf{s})] \end{pmatrix}. \tag{44}$$

Here, $\mathbb{A}$ is an 8×8 matrix with $A = \alpha^2$, $B = \alpha^2/(2\sqrt{1+\alpha^2})$, $C = 1+\alpha^2$, and $D = (1-\alpha^2)/(2\sqrt{1+\alpha^2})$. The solution $\mathbb{U}(t)$ is a

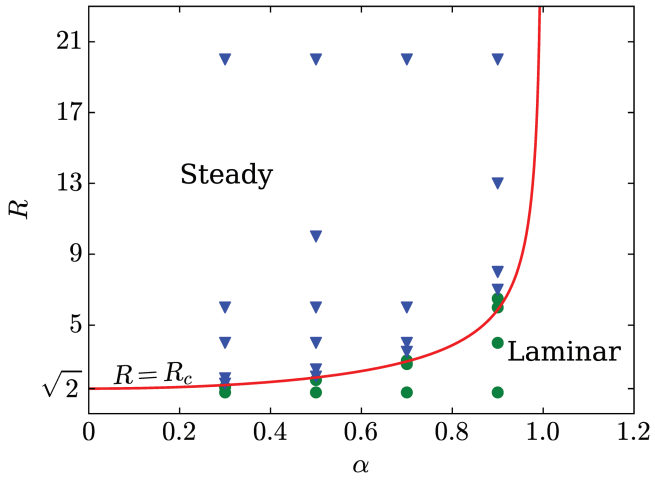

FIG. 3. Phase diagram (R, α) constructed using the $R = R_c$ curve, also called the neutral stability curve (the red curve). The figure also includes the steady-state results of the DNS. The green circles represent the laminar solution (S_0), but the blue triangles represent the steady vortex flow (S_1 or S_2).

linear combination of $e^{\lambda t}$, where λ's are the eigenvalues of $\mathbb{A}$,

$$\lambda_1 = -\frac{1}{R}, \tag{45}$$

$$\lambda_2 = -\frac{C}{R}, \tag{46}$$

$$\lambda_3 = -\frac{A + C + \sqrt{(A-C)^2 + 8BDR^2}}{2R}, \tag{47}$$

$$\lambda_4 = -\frac{A + C - \sqrt{(A-C)^2 + 8BDR^2}}{2R}. \tag{48}$$

It is easy to show that λ_1, λ_2, and λ_3 are negative for all α and R. However, λ_4 changes sign from negative to positive at the following condition, called the neutral stability condition,[40]

$$\sqrt{(A-C)^2 + 8BDR^2} = A + C \quad \text{or} \quad R = R_c, \tag{49}$$

where R_c is given by Eq. (34).

In Fig. 3, we exhibit the (R, α) phase diagram, the R_c curve, as well as the regions of stability and instability. As shown in the figure, R_c increases monotonically with α, and $R_c \to \infty$ as $\alpha \to 1$. Also, $R_c \to \sqrt{2}$ as $\alpha \to 0$. The figure shows that the system is stable below the $R = R_c$ curve and yields the laminar solution (S_0) and unstable otherwise. Note that for $\alpha > 1$, the laminar solution is stable for all R.

In Sec. III B, we show that for $\alpha < 1$ and $R > R_c$, the solutions S_1 and S_2 are the stable solutions.

B. Stability analysis of S_1 and S_2

As described in Sec. III, the solutions S_1, S_2 exist only for $r > 1$. In this subsection, we show that these are stable solutions for $r > 1$. For the stability analysis, we generate the stability matrix for S_1 and S_2 by linearizing Eqs. (27)–(30) around S_1, S_2. This exercise yields a set of equations for $\tilde{u}_1(\mathbf{k})$, $\tilde{u}_1(\mathbf{p})$, $\tilde{u}_1(\mathbf{q})$, and $\tilde{u}_1(\mathbf{s})$ similar to Eqs. (35)–(38). Note that $\tilde{u}_1(\mathbf{k})$, $\tilde{u}_1(\mathbf{p})$, $\tilde{u}_1(\mathbf{q})$, and $\tilde{u}_1(\mathbf{s})$ are fluctuations around S_1, S_2. The resulting matrix equation is

$$\frac{d}{dt}\mathbb{U} = \mathbb{B}\mathbb{U}, \tag{50}$$

where

$$\mathbb{B} = \begin{pmatrix} -\frac{A}{R} & 0 & 0 & \pm C' & D' & 0 & -D' & 0 \\ 0 & -\frac{A}{R} & 0 & 0 & 0 & -D' & 0 & D' \\ 0 & 0 & -\frac{1}{R} & 0 & 0 & \pm E' & 0 & \pm E' \\ \mp H' & 0 & 0 & -\frac{1}{R} & \pm E' & 0 & \mp E' & 0 \\ F' & 0 & 0 & \pm G' & -\frac{C}{R} & 0 & 0 & 0 \\ 0 & -F' & \pm G' & 0 & 0 & -\frac{C}{R} & 0 & 0 \\ -F' & 0 & 0 & \mp G' & 0 & 0 & -\frac{C}{R} & 0 \\ 0 & F' & \pm G' & 0 & 0 & 0 & 0 & -\frac{C}{R} \end{pmatrix}, \tag{51}$$

and C', D', E', F', G', and H' are $(AA')/R$, $(BR_c)/R$, $-(BA'R_c)/(AR)$, $(DR_c)/2R$, $(DA'R_c)/2R$, and A'/R, respectively. Here, $A' = \sqrt{(R/R_c) - 1}$, and A, B, C, D are the same as those defined in Sec. III A.

Similar to the stability analysis for S_0, we compute the eigenvalues of the matrix $\mathbb{B}$, which are

$$\lambda_1 = -\frac{C}{R}, \tag{52}$$

$$\lambda_2 = -\frac{1 + C + \sqrt{A + 8E'G'R^2}}{2R}, \tag{53}$$

$$\lambda_3 = -\frac{1 + C - \sqrt{A + 8E'G'R^2}}{2R}, \tag{54}$$

$$\lambda_4 = -\frac{A + C + \sqrt{1 + 8D'F'R^2}}{2R}, \tag{55}$$

$$\lambda_5 = -\frac{A + C - \sqrt{1 + 8D'F'R^2}}{2R}, \tag{56}$$

$$\lambda_6 = -\frac{2C}{3R} + \frac{2^{\frac{4}{3}} I' R}{6O} + \frac{2^{\frac{2}{3}} O}{6R^3}, \tag{57}$$

$$\lambda_7 = -\frac{2C}{3R} - \frac{2^{\frac{4}{3}} I' R(1 + \sqrt{3}i)}{12O} - \frac{2^{\frac{2}{3}} O(1 - \sqrt{3}i)}{12R^3}, \tag{58}$$

$$\lambda_8 = -\frac{2C}{3R} - \frac{2^{\frac{4}{3}} I' R(1 - \sqrt{3}i)}{12O} - \frac{2^{\frac{2}{3}} O(1 + \sqrt{3}i)}{12R^3}. \tag{59}$$

In the above expressions, I' and O are complicated functions of α and R; hence, they are not presented here. The eigenvalues $\lambda_1, \lambda_2, \lambda_3, \lambda_4, \lambda_5$ are always real and negative. However, λ_6, λ_7, λ_8 could become complex, and still their real parts are always negative. Thus, we demonstrate that the solutions S_1, S_2 are stable for $r > 1$ for which these solutions are defined. Using these observations, we also conclude that the transition at $r = 1$ (or $R = R_c$) follows a supercritical pitchfork bifurcation, as illustrated in Fig. 2 for $\alpha = 0.7$.

In Fig. 4, we illustrate the flow profile of the vortex pattern generated by the modes of S_1 for $\alpha = 0.7$ and $R = 4.61$. Note that the large-scale vortical flow results from the presence of all the

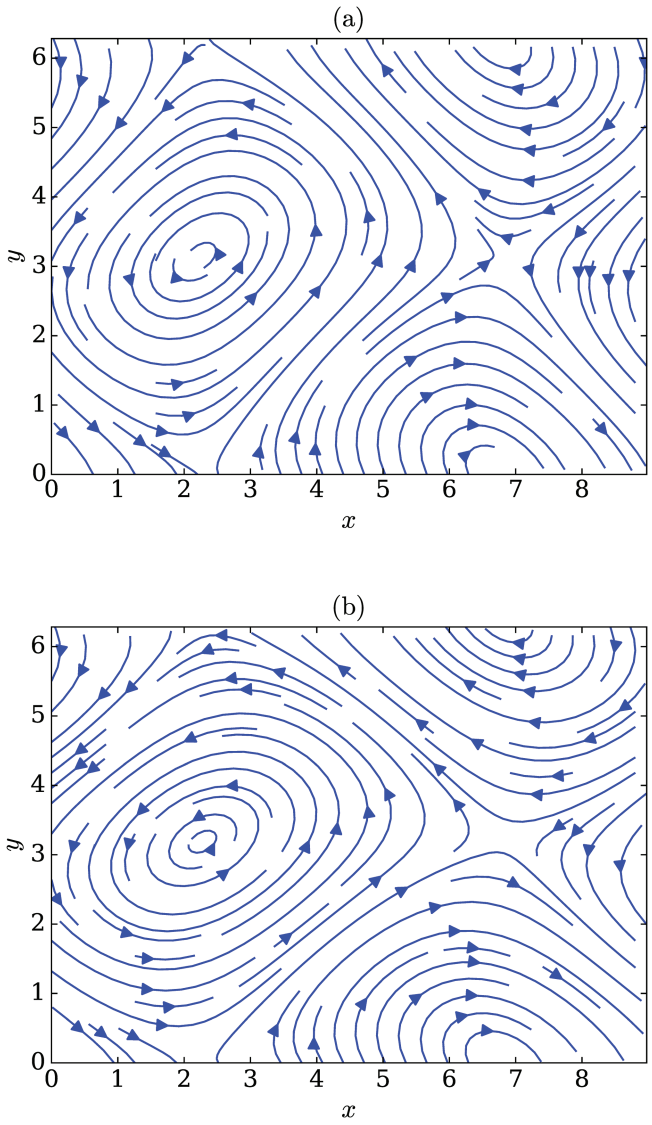

FIG. 4. (a) The flow patterns for the model solution S_1 with $\alpha = 0.7$ and $R = 4.61$. Here, $L_x = 2\pi/\alpha$ and $L_y = 2\pi$. (b) The same steady flow pattern, is observed in DNS for the same parameters.

four modes of the model. Interestingly, the vortical flow pattern is very similar to those presented in earlier works, e.g., Okamoto and Shōji.[11] Note that $R_c = 2.95$ for $\alpha = 0.7$.

The bifurcation mentioned above indicates that for $\alpha < 1$, Fourier modes with large wavelengths get excited. In Sec. IV, we will describe energy transfers among the interacting Fourier modes.

IV. ENERGY TRANSFERS IN THE KOLMOGOROV FLOW

In this section, we will quantify the energy transfers between the interacting Fourier modes $\mathbf{u}(\mathbf{k})$, $\mathbf{u}(\mathbf{p})$, $\mathbf{u}(\mathbf{q})$, and $\mathbf{u}(\mathbf{s})$. For the same, we will employ the mode-to-mode energy transfer formalism proposed by Dar, Verma, and Eswaran[41] and Verma.[42] For triad (**k**,**p**,**q**) satisfying **k**+**p**+**q** = 0, the energy transfer from $\mathbf{u}(\mathbf{p})$ to $\mathbf{u}(\mathbf{k})$ with the mediation of $\mathbf{u}(\mathbf{q})$ is

$$S^{uu}(\mathbf{k}|\mathbf{p}|\mathbf{q}) = -\Im[\{\mathbf{k}\cdot\mathbf{u}(\mathbf{q})\}\{\mathbf{u}(\mathbf{p})\cdot\mathbf{u}(\mathbf{k})\}]. \tag{60}$$

For the transfers between other Fourier modes, we employ the corresponding giver, receiver, and mediator Fourier modes.

For the laminar solution S_0, energy transfers among the Fourier modes vanish due to a lack of a nonzero interacting triad. For S_1, S_2, there is no energy exchange between the Fourier modes $\mathbf{u}(\mathbf{k})$ and $\mathbf{u}(\mathbf{p})$, that is,

$$S^{uu}(\mathbf{k}|\mathbf{p}|\mathbf{q}) = 0. \tag{61}$$

However, there are energy transfers among other Fourier modes. They are

$$S^{uu}(\mathbf{k}|\mathbf{q}|\mathbf{p}) = S^{uu}(-\mathbf{k}|-\mathbf{s}|\mathbf{p}) = \gamma = \frac{\alpha^2(r-1)}{4\sqrt{2}Rr^2}, \tag{62}$$

$$S^{uu}(\mathbf{q}|\mathbf{p}|\mathbf{k}) = S^{uu}(-\mathbf{s}|\mathbf{p}|-\mathbf{k}) = \sigma = \frac{(r-1)}{4\sqrt{2}Rr^2}. \tag{63}$$

It is evident that γ and σ are positive because $r > 1$. Also, $\sigma > \gamma$ because $\alpha < 1$. These energy transfers are illustrated in Fig. 1.

The energy transfer computations indicate that the velocity mode $\mathbf{u}(0,1)$ gives energy to $\mathbf{u}(\alpha,-1)$, which in turn gives energy to $\mathbf{u}(\alpha,0)$. Since $\alpha < 1$, the wavenumber $(\alpha,0)$ yields the largest wavelength. Thus, the energy flows from the intermediate scale [corresponding to the wavenumber (0,1)] to the large scale [corresponding to the wavenumber $(\alpha,0)$]. Hence, we conclude that the Kolmogorov flow exhibits an inverse energy cascade, contrary to the forward energy transfer observed in three-dimensional hydrodynamic turbulence.

In Sec. V, we will describe results from direct numerical simulation and compare them with the results of the low-dimensional model.

V. COMPARISON WITH DIRECT NUMERICAL SIMULATIONS

In this section, we will compare the results of direct numerical simulation (DNS) of the Kolmogrov flow with the model results. We numerically solve Eqs. (4) and (5) using the pseudospectral method in the domain $[0, 2\pi/\alpha] \times [0, 2\pi]$ with periodic boundary conditions on all sides. We discretize the domain into 64^2 uniform grid points. We start the simulation with the initial condition, $\{u_1(\mathbf{k}), u_1(\mathbf{p}), u_1(\mathbf{q}), u_1(\mathbf{s})\} = \{-0.01, 0.01, -0.01(\sqrt{1+\alpha^2}/\alpha), 0.01(\sqrt{1+\alpha^2}/\alpha)\}$, with negative wavenumber modes given by the corresponding complex conjugates. The rest of the modes are zeros. We employ RK2 (second order Runge–Kutta) scheme for time advancement with a fixed time step $dt = 0.01$. We employ the 2/3 rule for dealiasing.

We perform the 30 runs for different values of $\{\alpha, R\}$, which are displayed in Fig. 3 as green circles and blue triangles. We observe that all the simulations reach steady solutions, which are either laminar solutions (S_0, green dots) or vortex solutions (S_1 or S_2, blue triangles). Note that the two sets of simulations are nearly separated

TABLE I. For $\alpha = 0.7$ and $R = 4.61$, the relative amplitudes of the modes of the low-dimensional model (LDM), as well as the relative amplitudes of the dominant modes of DNS. The total energy of the DNS is 0.188 and that for LDM is 0.18. The amplitudes are for the steady state at $t = 440$. This table does not include the $-\mathbf{k}$ modes that contain the remaining 50% of the total energy.

$\mathbf{k} = (k_x, k_y)$	$E(\mathbf{k})/E(\%)$ (DNS)	$E(\mathbf{k})/E(\%)$ (LDM)
$(\alpha, 0)$	16.035	15.975
$(0, 1)$	29.459	28.563
$(\alpha, 1)$	2.197	2.731
$(\alpha, -1)$	2.197	2.731
$(2\alpha, 1)$	0.053	...
$(-2\alpha, 1)$	0.053	...
$(2\alpha, 2)$	0.002	...
$(3\alpha, 1)$	0.001	...
$(\alpha, 2)$	0.001	...

by the $R = R_c$ curve, which is the red curve in Fig. 3. These observations indicate that our low-dimensional model captures the DNS results very well for the parameters of Fig. 3.

The dominant Fourier modes of the DNS are the same as those of the low-dimensional model. The other modes have much small magnitudes. The flow profiles of the DNS and the model are very similar, consistent with the above observations. For example, for the parameter values, $\alpha = 0.7$ and $R = 4.61$, the steady-state flow profiles of the low-dimensional model and DNS exhibited in Fig. 4 are very similar. For the same parameter values, the steady-state values of the dominant Fourier modes for the DNS and the low-dimensional model are quite close to each other (see Table I). For the DNS, the nine modes (along with their complex conjugates) listed in Table I contain nearly all of the total energy of the system.

In our DNS, we do not observe solutions other than S_0, S_1, and S_2. That is, we do not observe any secondary bifurcation in our simulations. The DNS for $\alpha = 0.7$ and $R = 200$ too exhibits a steady vortical flow structure as in Fig. 4, thus indicating the absence of a secondary bifurcation. Note, however, that Okamoto and Shōji[11] had predicted secondary bifurcations for $\alpha = 0.98$, as well as on the unstable branch for $\alpha = 0.35$. These are specialized cases that require special initial conditions and careful time-advancing of the DNS; hence, this investigation is deferred for future.

For the computation of the energy spectrum and flux, we performed a DNS for $\alpha = 0.7$ and $R = 200$ on a relatively higher resolution of 512^2. We obtain a steady flow at $t = 1300$; at this time, the energy spectrum $E(k)$ is very steep. The steep power law of k^{-7} provides a reasonable fit to the energy spectrum, which is consistent with the predictions of Okamoto.[13] We also remark that the exponential function $\exp(-2.5k)$ too provides a reasonable fit to the spectrum; this result is consistent with the arguments that the low-dimensional systems and the dissipation range of turbulent flows exhibit an exponential spectrum.[43,44] Note that Zhang *et al.*[28] obtained similar scaling in their simulation of the Kolmogorov flow. See Fig. 5(a) for an illustration.

We also compute the energy flux $\Pi(k)$ for the same run. The energy flux is negative for the smallest wavenumber sphere of radius 0.5, indicating an inverse cascade of energy [see Fig. 5(b)]. The

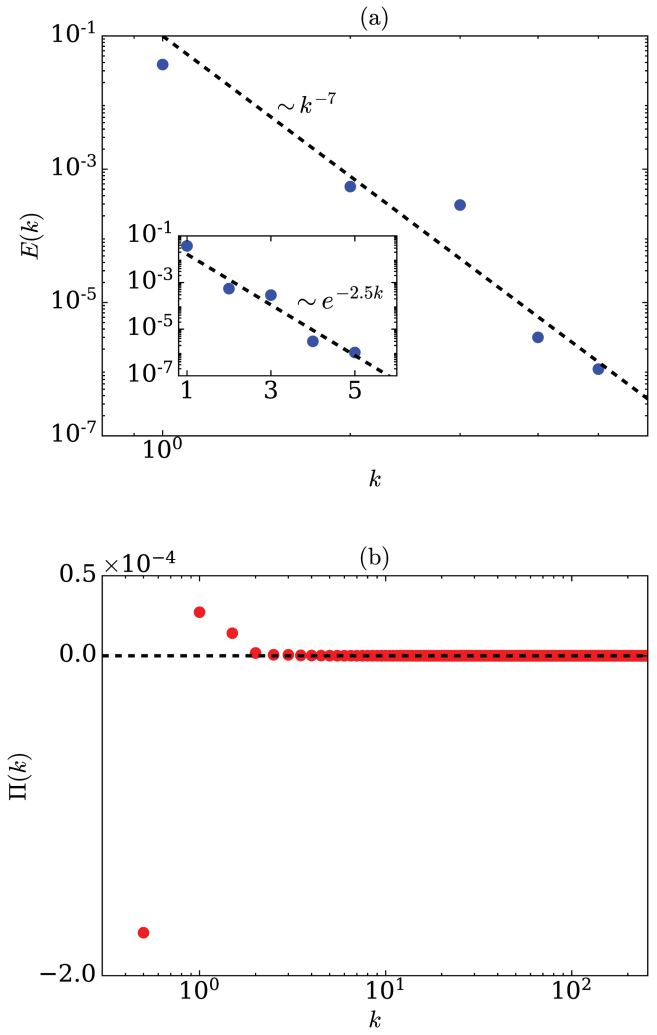

FIG. 5. For DNS with $\alpha = 0.7$ and $R = 200$: (a) the energy spectrum $E(k)$ and (b) the energy flux $\Pi(k)$. Both power law (k^{-7}) and exponential function [$\exp(-2.5k)$] [see the inset of (a)] fit with the numerical data reasonably well. $\Pi(k)$ is negative for the lowest wavenumber, indicating an inverse cascade. Also, $\Pi(k)$ is negligible for $k > 3$ due to the dominance of small wavenumber modes.

simulation result is close to the model result, that is, the energy transfer from $u_1(-\alpha, -1)$ to $u_1(\alpha, 0)$ shown in Fig. 1 and discussed in Sec. IV. In addition, $\Pi(k)$ falls sharply. Thus, both the energy spectrum and the flux support earlier observations that only small wavenumber modes are active in the Kolmogorov flow. For example, see Table I.

We conclude in Sec. VI.

VI. DISCUSSIONS AND CONCLUSIONS

In this paper, we present a low-dimensional model that captures the essential features of the Kolmogorov flow. The Fourier components are in the Craya–Herring basis. We identify the fixed

points of the system and show that the system bifurcates from the laminar solution to a new solution with the vortex structure. These solutions are consistent with earlier works based on analytical, numerical, and experimental tools. In addition, we perform direct numerical simulation (DNS) of the Kolmogorov flow that exhibits similar results as the low-dimensional model.

Our low-dimensional model captures the critical Reynolds number of the Kolmogorov flow. The model predicts that the new vortex solution remains stable beyond $R > R_c$. The critical Reynolds number R_c increases monotonically with α, with $R_c \to \sqrt{2}$ as $\alpha \to 0$ and $R_c \to \infty$ as $\alpha \to 1$. However, between these two limits, the model prediction of R_c is marginally lower than those computed using models containing a larger number of Fourier modes.[11,12] Using energy transfers, we show that in the Kolmogorov flow, the energy flows from intermediate scales to large scales; this is contrary to the forward energy transfers in Kolmogorov's theory of turbulence. Thus, our model captures essential aspects of the primary bifurcation of the Kolmogorov flow, and its results are consistent with earlier models.

Our DNS results are very similar to those of the low-dimensional model. For example, the flow patterns and the dominant modes of DNS are close to those of the low-dimensional model. Both DNS and the model do not exhibit any secondary bifurcation, indicating the robustness of the low-dimensional model. It is interesting to note that the six-mode dynamo model of Verma *et al.*[45] showed very similar bifurcation, as described in this paper. It is possible that the Kolmogorov flow with forcing at larger wavenumbers ($k_f > 1$) may exhibit secondary bifurcation.

There are certain discrepancies between the predictions of our model and those of earlier models. As shown by Okamoto and Shōji,[11] we expect secondary bifurcations for α very close to unity, as well as on the unstable branch for other α's. A verification of Okamoto and Shōji's[11] predictions on secondary bifurcations using DNS requires major fine-tuning of the initial conditions and the DNS, and it is planned for the future. Also, our model does not capture several oscillatory solutions predicted by Sivashinsky.[9] These issues need to be explored in the future.

In summary, our four-mode model captures many of its interesting features of the Kolmogorov flow. It also opens avenues for further explorations of the Kolmogorov flow with $k_f > 1$ and large Reynolds numbers.

ACKNOWLEDGMENTS

We thank Roshan Samuel, Shashwat Bhattacharya, Mohammad Anas, Narendra Pratap, Akanksha Gupta, Shadab Alam, and Manohar Sharma for useful discussions. This work was supported by the research grant (No. 6104-1) from the Indo-French Centre for the Promotion of Advanced Research (IFCPAR/CEFIPRA). Soumyadeep Chatterjee is supported by the INSPIRE fellowship (No. IF180094) of the Department of Science & Technology, India.

DATA AVAILABILITY

The data that support the findings of this study are available from the corresponding author upon reasonable request.

REFERENCES

[1] V. I. Arnol'd and L. D. Meshalkin, "A. N. Kolmogorov's seminar on selected problems of analysis (1958–1959)," Usp. Mat. Nauk **15**, 247–250 (1960).
[2] A. M. Obukhov, "Kolmogorov flow and laboratory simulation of it," Russ. Math. Surv. **38**, 113–126 (1983).
[3] V. I. Arnol'd, "Kolmogorov's hydrodynamic attractors," Proc. R. Soc. A: Math. Phys. Eng. Sci. **434**, 19–22 (1991).
[4] J. M. Burgess, C. Bizon, W. D. McCormick, J. B. Swift, and H. L. Swinney, "Instability of the Kolmogorov flow in a soap film," Phys. Rev. E **60**, 715 (1999).
[5] N. F. Bondarenko, M. Z. Gak, and F. V. Dolzhanskii, "Laboratory and theoretical models of plane periodic flow," Akad. Nauk SSSR Izv. Fiz. Atmosfery Okeana **15**, 1017–1026 (1979).
[6] B. Suri, J. Tithof, R. Mitchell, R. O. Grigoriev, and M. Schatz, "Velocity profile in a two-layer Kolmogorov like flow," Phys. Fluids **26**, 053601 (2014).
[7] L. D. Meshalkin and Y. G. Sinai, "Investigation of the stability of a stationary solution of a system of equations for the plane movement of an incompressible viscous liquid," J. Appl. Math. Mech. **25**, 1700–1705 (1961).
[8] V. I. Iudovich, "Example of the generation of a secondary stationary or periodic flow when there is loss of stability of the laminar flow of a viscous incompressible fluid," J. Appl. Math. Mech. **29**, 527–544 (1965).
[9] G. I. Sivashinsky, "Weak turbulence in periodic flows," Physica D **17**, 243–255 (1985).
[10] C. Marchioro, "An example of absence of turbulence for any Reynolds number," Commun. Math. Phys. **108**, 647–651 (1987).
[11] H. Okamoto and M. Shōji, "Bifurcation diagrams in Kolmogorov's problem of viscous incompressible fluid on 2-D flat tori," Jpn. J. Ind. Appl. Math. **10**, 191–218 (1993).
[12] K. Nagatou, "A computer-assisted proof on the stability of the Kolmogorov flows of incompressible viscous fluid," J. Comput. Appl. Math. **169**, 33–44 (2004).
[13] H. Okamoto, "Nearly singular two-dimensional Kolmogorov flows for large Reynolds numbers," J. Dyn. Differ. Equ. **8**, 203–220 (1996).
[14] H. Okamoto, "A study of bifurcation of Kolmogorov flows with an emphasis on the singular limit," Doc. Math. J. DMV Extra Vol. ICM **3**, 513–522 (1998).
[15] M. Matsuda and S. Miyatake, "Bifurcation analysis of Kolmogorov flows," Tohoku Math. J. **54**, 329–365 (2002).
[16] P. Tabeling, B. Perrin, and S. Fauve, "Instability of a linear array of forced vortices," Europhys. Lett. **3**, 459–465 (1987).
[17] J. Sommeria, "Experimental study of the two-dimensional inverse energy cascade in a square box," J. Fluid Mech. **170**, 139–168 (1986).
[18] J. Herault, F. Pétrélis, and S. Fauve, "Experimental observation of 1/f noise in quasi-bidimensional turbulent flows," Europhys. Lett. **111**, 44002 (2015).
[19] P. Tabeling, "Two-dimensional turbulence: A physicist approach," Phys. Rep. **362**, 1–62 (2002).
[20] K. Gotoh and M. Yamada, "The instability of rhombic cell flows," Fluid Dyn. Res. **1**, 165–176 (1987).
[21] S. C. Kim and H. Okamoto, "Bifurcations and inviscid limit of rhombic Navier-Stokes flows in tori," IMA J. Appl. Math. **68**, 119–134 (2003).
[22] A. Thess, "Instabilities in two-dimensional spatially periodic flows. I. Kolmogorov flow," Phys. Fluids A **4**, 1385–1395 (1992).
[23] N. Platt, L. Sirovich, and N. Fitzmaurice, "An investigation of chaotic Kolmogorov flows," Phys. Fluids A **3**, 681 (1991).
[24] Z. M. Chen and W. G. Price, "Chaotic behavior of a Galerkin model of a two-dimensional flow," Chaos **14**, 1056 (2004).
[25] I. E. Sarris, H. Jeanmart, D. Carati, and G. Winckelmans, "Box-size dependence and breaking of translational invariance in the velocity statistics computed from three-dimensional turbulent Kolmogorov flows," Phys. Fluids **19**, 095101 (2007).
[26] J. S. A. Green, "Two-dimensional turbulence near the viscous limit," J. Fluid Mech. **62**, 273–287 (1974).
[27] A. Gupta, R. Jayaram, A. G. Chaterjee, S. Sadhukhan, R. Samtaney, and M. K. Verma, "Energy and enstrophy spectra and fluxes for the inertial-dissipation range of two-dimensional turbulence," Phys. Rev. E **100**, 053101 (2019).
[28] J. Zhang, P. Tian, S. Yao, and F. Fei, "Multiscale investigation of Kolmogorov flow: From microscopic molecular motions to macroscopic coherent structures," Phys. Fluids **31**, 082008 (2019).

[29]B. Gallet and W. R. Young, "A two-dimensional vortex condensate at high Reynolds number," J. Fluid Mech. **715**, 359–388 (2013).
[30]P. K. Mishra, J. Hérault, S. Fauve, and M. K. Verma, "Dynamics of reversals and condensates in two-dimensional Kolmogorov flows," Phys. Rev. E **91**, 053005 (2015).
[31]G. J. Chandler and R. R. Kerswell, "Invariant recurrent solutions embedded in a turbulent two-dimensional Kolmogorov flow," J. Fluid Mech. **722**, 554–595 (2013).
[32]D. Lucas and R. Kerswell, "Spatiotemporal dynamics in 2D Kolmogorov flow over large domains," J. Fluid Mech. **750**, 518–554 (2014).
[33]E. Fylladitakis, "Kolmogorov flow: Seven decades of history," J. Appl. Math. Phys. **6**, 2227–2263 (2018).
[34]M. K. Verma, *Physics of Buoyant Flows: From Instabilities to Turbulence* (World Scientific, Singapore, 2018).
[35]M. K. Verma, *Energy Transfers in Fluid Flows: Multiscale and Spectral Perspectives* (Cambridge University Press, Cambridge, 2019).
[36]A. Craya, "Contribution à l'analyse de la turbulence associée à des vitesses moyennes," Ph.D. thesis (School Université de Granoble, 1958).
[37]J. R. Herring, "Approach of axisymmetric turbulence to isotropy," Phys. Fluids **17**, 859–872 (1974).
[38]M. Lesieur, *Turbulence in Fluids* (Springer-Verlag, Dordrecht, 2008).
[39]P. Sagaut and C. Cambon, *Homogeneous Turbulence Dynamics*, 2nd ed. (Cambridge University Press, Cambridge, 2018).
[40]S. Chandrasekhar, *Hydrodynamic and Hydromagnetic Stability* (Oxford University Press, Oxford, 2013).
[41]G. Dar, M. K. Verma, and V. Eswaran, "Energy transfer in two-dimensional magnetohydrodynamic turbulence: Formalism and numerical results," Physica D **157**, 207–225 (2001).
[42]M. K. Verma, "Statistical theory of magnetohydrodynamic turbulence: Recent results," Phys. Rep. **401**, 229–380 (2004).
[43]S. Paul, P. K. Mishra, M. K. Verma, and K. Kumar, "Order and chaos in two-dimensional Rayleigh-Bénard convection," arXiv:0904.2917 (2009).
[44]A. Bershadskii, "Near-dissipation range in nonlocal turbulence," Phys. Fluids **20**, 085103 (2008).
[45]M. K. Verma, T. Lessinnes, D. Carati, I. E. Sarris, K. Kumar, and M. Singh, "Dynamo transition in low-dimensional models," Phys. Rev. E **78**, 036409 (2008).